Machine Copy for Proofreading, Vol. x, y–z, 2012

SIMPLE TRAFFIC SURVEILLANCE SYSTEM BASED ON RANGE-DOPPLER RADAR IMAGES

J. Calvo-Gallego[1, *] and F. Pérez-Martínez[2]

[1]Department of Computing and Automatics, University of Salamanca, Avda. Requejo, 33, 49022, Zamora, Spain

[2]Department of Signals, Systems and Radiocommunications, Technical University of Madrid, Avda. Complutense, s/n, Madrid 28040, Spain

Abstract—A simple traffic surveillance system based on the extraction of features from range-Doppler radar images is addressed. The concept exploits the High-Resolution Radars (HRR) properties. Specifically, it is proposed a procedure to obtain some features from the HRR non-cooperative targets to enable their classification. These features are: the distance, radial velocity and radial longitudinal dimension of the target; its integrated range-Doppler image based on a group of range-Doppler frames from each target, and both the coherent and non-coherent integrated range profiles. Experimental results from real scenarios using a high-resolution Linear-Frequency-Modulated Continuous-Wave (LFMCW) millimetre-wave radar are shown.

1. INTRODUCTION

Many years ago, the requirements to be met by a sensor in order to carry out tasks of detection, classification and identification were defined. Perhaps, one of the most remarkable criteria is found in [1] and described in [2], where the minimum number of lines needed for these tasks were specified. Unfortunately, these definitions are not applicable today for the current High–Resolution Radars (HRR) [3].

The output data for a HRR may be a one-, two- or three-dimensional array, depending on the HRR sensor. This feature makes it possible to extrapolate all the techniques available in the field of Digital Image Processing (DIP) [4], to the images captured by the HRR sensors. Even colour techniques developed in DIP are applicable

Received 18 January 2012.

* Corresponding author: Jaime Calvo-Gallego (jaime.calvo@usal.es).

to HRR data, for obtaining, as an example, multiple images of the same scene, by using different frequency bands, or for making use of several frames from the acquired radar targets. The present paper concentrates on the latter, by using a sequence of range-Doppler radar images from each target.

Non-coherent radars are only able to obtain range profiles (one-dimensional arrays), whereas coherent radar may obtain range-Doppler images (two-dimensional images). 3-D coherent radar (perhaps with steering capability in elevation) could obtain three-dimensional images.

With the current characteristics of HRR sensors, it is not possible to carry out the univocal identification of most objects, especially the smaller ones, because there is not enough resolution. For example, it is possible to distinguish a car from a bus or from a motorcycle, but it is very difficult to distinguish several cars of different models.

In a scenario characterized by a limited number of targets of sufficient size (several tens of pixels in each range profile) and/or targets having very different size, it may be possible to identify each target present in the scene. In fact, we have made some experiments with HRR sensors that allow us to ensure that, for example, in a battle with ships of war, these HRR sensors can quickly identify any warfare ship platform, by the method of estimating their lengths and the intensity of received back-scattered signal.

In any case, the data provided by HRR sensors could be used to complement other sensors (visible cameras, infrared vision cameras, etc.). Of course, databases containing signatures from different types of clutter and targets may also help in this task. Nevertheless, the ultimate identification of a particular car requires reading the vehicle registration plate with an electro-optical sensor, but it is possible to think of a system in which the camera is pointing to that target (among many others) after a pre-classification process based on HRR sensors.

Almost all the developed algorithms for identification purposes in radar images have been developed for specific systems and well defined applications, without a valid general theory to perform the identification in any general framework; and obviously it is not feasible to develop a unique algorithm to carry out the identification tasks of all kinds of targets under any clutter conditions and at any operational environment application. Some examples of algorithms developed for specific sensors operating in specific applications have mainly been developed for SAR (Synthetic Aperture Radar) [5–7], and ISAR (Inverse SAR) [8, 9]. Other examples, reference [10] proposes a method for identifying boundaries of water basins, and polygonal patterns in noisy SAR images. A method of identification for a specific sensor system, with the aim of identifying land movements in a particular

geographical environment, is provided in [11]. In [12], it is addressed the issue of target classification to a level close to the identification. In [13], the basis for the automatic interpretation of images from sensors in general is approached, proposing a systematic approach to the interpretation of the scene present in the sensed image by the sensors. The results are applied to restoration of high-resolution SAR images.

This paper presents a simple computationally-efficient strategy for feature extraction of non-cooperative targets detected by HRR sensors. The purpose is to classify targets on various types of traffic scenarios: road, marine, and air traffic. Some examples of specific techniques developed in this field could be found in [14–23]. The proposed technique is based on the extraction of several descriptors, for each target, from sequences of range-Doppler images [24], such as the radial length, the dynamics, two range-Doppler integrated image (coherent and non-coherent), and the range profiles integrated in Doppler (coherent and non-coherent). The application of the proposed technique is well suited for non-cooperative targets. However, note that target aspect angles are assumed to be known. In this way, the measured lengths and Doppler may be easily corrected to obtain real target dimensions and speeds.

Experimental results from real scenarios using a high-resolution Linear-Frequency-Modulated Continuous-Wave (LFMCW) millimetre-wave radar prove the viability of the proposed traffic surveillance system [25, 26].

2. TARGET CLASSIFICATION BASED ON HIGH-RESOLUTION RANGE-DOPPLER RADAR IMAGES

The inherent difficulty of the classification techniques, together with the fact that they also require a better Signal-to-Noise Ratio (SNR) than detection and localization stages, suggest the desire to integrate the information contained in a set of range-Doppler images, instead of using just one. The high-resolution radars have such ability.

The monitoring system proposed here is based on performing a classification of non-cooperative targets based on range-Doppler images obtained with a high-resolution radar operating in tracking mode.

When the sensor provides coherent data (this means, with phase information), as is the case of the real HRR sensor in millimetre-band, and working in tracking mode, then it is immediate to compute the range-Doppler image. The range dimension provides the information of the hot spots (also called peak plots) of the target in range [27], whereas

the Doppler dimension provides information about the movement of these hot spots. Also, it is important to note that the range resolution is limited, and that Doppler spreading caused by the migration through resolution cells usually arises [28].

The two radar image dimensions are range (slant-range: radar signal over the Line-Of-Sight (LOS)) and Doppler (simply related to cross-range). High range resolution is achieved by transmitting a large bandwidth signal, and high Doppler resolution depends on a large aspect angle variation of the target during the illumination time (or dwell time) [26]. The range resolution is given by

$$\rho_r = \frac{c}{2\Delta f}, \tag{1}$$

where c is the light speed and Δf is the transmitted bandwidth. The Doppler resolution is given by

$$\rho_D = \frac{1}{t_{ilum}}, \tag{2}$$

where t_{ilum}, illumination time, is the time during a scatter stays within the same range resolution cell. Then

$$t_{ilum} = \frac{\rho_r}{v_r}, \tag{3}$$

where v_r is the radial velocity of the target. Thus, the Doppler resolution is inversely proportional to the time in which the scatter remains in a range resolution cell. If there is slant range migration, then the time decreases and the Doppler resolution is degraded.

Experiments show that it is possible to make the assumption that each scatterer from the target has a similar movement, which explains why, considering the dynamics of the maximum value or the centroid of the target, you can infer its dynamics. However, if the target has a rotational movement in a proper plane, we can estimate the position of the scatters (if the rotational velocity of the target is known or can be computed) by means of the different Doppler frequency produced by each of them.

The obtained range-Doppler radar image is an Inverse Synthetic Aperture Radar image, which is a projected image depending on both target dynamics and its relative orientation with regards to the radar.

The ISAR projection plane is a plane formed by the LOS vector and the vector normal to the effective rotation vector of the target (which is the projection of the rotation vector over the plane perpendicular to the LOS), and contained in the plane perpendicular to LOS [29].

In a simple way, it is possible to divide the target motion into two components: a translational and a rotational component. The former

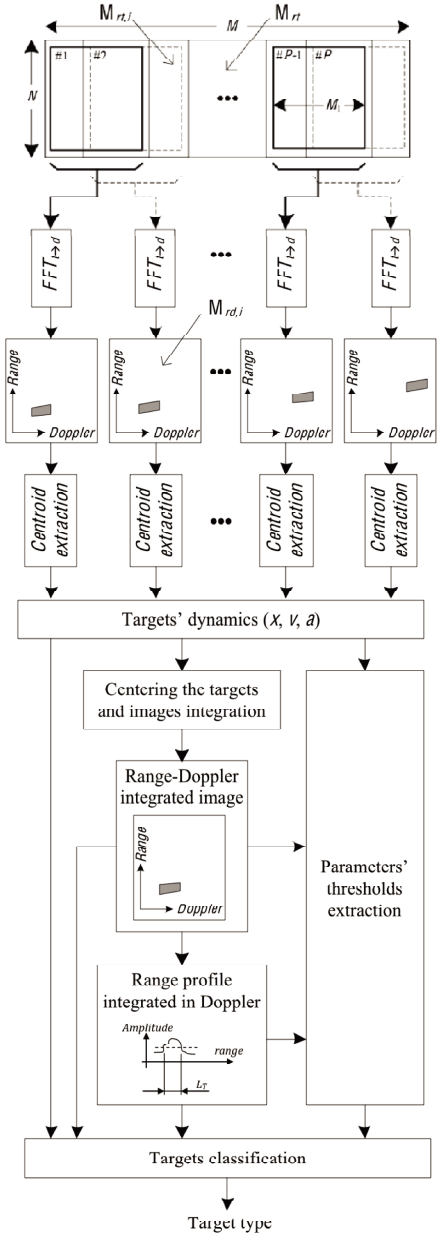

Figure 1. Block diagram of the target classification technique for traffic surveillance.

is the component along the LOS of the translational motion of the target and it is an undesired component, since it does not generate Doppler gradient among scatterers of the target placed in the same range cell. However, the latter may generate the desired Doppler gradient among scatterers located in the same range cell. This fact allows distinguishing between several scatters placed within the same resolution cell.

3. PROPOSED TRAFFIC-SURVEILLANCE SYSTEM

Figure 1 shows the block diagram of the proposed technique. After deciding the beginning of the capture and processing of the radar signal, the sequence of range-Doppler images are being obtained. Each complete radar capture, the slow-time vs. fast-time matrix is formed, which is divided into smaller areas. Specifically, by dividing this data matrix in slow-time dimension, a sequence of range-Doppler images is obtained. Each range-Doppler image is transferred to the detection process (e.g., CFAR for high-resolution radars, or another one). Then, the target dynamics' is computed. From the sequence of range-Doppler images, the dynamics of each target may be obtained (computing the position, $\mathbf{x}$, velocity, $\mathbf{v}$, and acceleration, $\mathbf{a}$). In fact, the measured velocity is the radial velocity, v_r, of the target, but is straightforward to compute the real velocity making use of the relative aspect angles in azimuth and elevation.

Subsequently, for each target, a centred and aligned integration of the entire sequence of range-Doppler images is performed. To do so, a superposition of the entire sequence of images is made, previously extracting the centroids of the target in each image, and aligning the target in all the Images by the centroid and the aspect angle (angle between the line-of-sight, LOS, and the line that defines the maximum dimension of target). The resulting image is called the range-Doppler integrated image.

The integration of range-Doppler images is performed in two ways: coherent (considering modulus and phase of the signal), and non-coherent (only considering the signal amplitude). The former is called I-Q range-Doppler integrated image, and the latter is called the non-coherent range-Doppler integrated image. From these obtained integrated images, in turn, two range profiles integrated in Doppler were computed (resulting from the sum of all values of the Doppler bins, for each of the range bins): coherent and non-coherent, for each one of the two kinds of integrated range-Doppler images, also called the I-Q integrated range profile, and the non-coherent integrated range profile, respectively.

From the integrated range profile, it can be estimated the transverse length of the target (the main length), L_T. All these data are stored and processed in the thresholds extraction block for classification purposes. For example, in a road traffic surveillance application, the classification thresholds "x-type car" may be: maximum and minimum distance (within the range in which the road exists), maximum and minimum speed (if into the section under surveillance it is feasible to define the range of the allowed speed limits), maximum and minimum target length (this may be the most reliable parameter), and finally, the pattern of the association algorithm from the integrated range profiles, and the integrated range-Doppler images.

The next steps describe the algorithm of the proposed simple traffic surveillance system based on range-Doppler radar images:

- **Step 1.** Generate the range-slow time matrix M_{rt} from the radar data.
- **Step 2.** Generate the range-Doppler matrix M_{rd} via FFT in the t-dimension of M_{rt}. Obtaining a set of range-Doppler images.
- **Step 3.** Isolate the echoes of each vehicle in the matrix M_{rd}.
- **Step 4.** Compute the targets' dynamics, obtaining the position, **x**, the radial velocity, **v**, and the acceleration, **a**, from the set of range-Doppler images sequence of the same target.
- **Step 5.** Estimate the centroid for each target in the sequence $M_{rd,i}$, in each range-Doppler radar image of the image sequence for the same target.
- **Step 6.** For each target, the range-Doppler integrated image is obtained by centring and aligning each range-Doppler matrix, $M_{rd,i}$, and making the sum in two different ways. The first one through a coherent sum (taking in mind both the real and the imaginary part of the signal); and the second one, just considering the modulus of the signal. (The I-Q range-Doppler integrated image, and the non-coherent range-Doppler integrated image, respectively).
- **Step 7.** From the previous step, the range profile integrated in Doppler making the sum of each range profile of the range-Doppler integrated image is computed. Also, in this step, the sum is carried out in two ways, first, in a coherent way, for I-Q range-Doppler integrated image (the I-Q integrated range profile); and second in a non-coherent way, for the non-coherent range-Doppler integrated image (the non-coherent integrated range profile).
- **Step 8.** A set of thresholds are computed from the information of the targets' dynamics, of the range-Doppler integrated image, and of the range profile integrated in Doppler, in order to get an

estimation of the characteristic parameters of the targets, i.e., the estimated length of the target, L_T.

- **Step 9.** By grouping the previous information about the target, it is possible to carry out a classification of each target according to the parameters of each one of them, obtaining the target type.

This system also could be considered as open traffic-surveillance architecture, in other words, the presented block diagram, Figure 1, allows to build-in other kinds of specific techniques of classification [30], recognition [31–35], identification techniques [36, 37], and could be complemented with other tracking algorithms as [38–41]. In the same way, the architecture could be successfully applied to different scenarios. As an example, for target localization with unknown wall parameters for through-the-wall radar imaging applications, it is strongly recommended to implement the novel approach to correct the shift in target position due to the ambiguities of the wall parameters presented in [42]. Other example could be the classification of dielectric scatters to distinguish between malignant and benign tumours within breast cancer applications, as suggested in [43, 44]. In this case, our scheme should be complemented with one of the different combinations of tumour classifiers, analysed in this reference.

3.1. Target Modelling

From a simple model of target, the maximum achievable precisions and the influence on them due to the parameters selection of the HRR sensor were obtained. For these issues, we have chosen to synthesize a target consisting of two point scatterers separated by a known distance. The mathematical details of the simulation can be found in [3]. Highlights of the used target modelling are described below.

Based on the integrated range profiles, a measure of the target lengths was performed, in order to extract another identifying characteristic from these ones. This measure, together with the rest of extracted parameters, allows the development of classification stages of targets for traffic surveillance purposes. Of course, these kinds of profiles can be used in many other classification techniques.

As for the method to determine the length of the target, in the parametric studies, carried out on the target modelled as two point scatterers, we have made the choice to measure the distance between the two highest level scatterers in the integrated range profile, due to the composition of that target. Then, this measure of the distance is the length of the target modelled as two point scatters. The goal of this method of length measurement is to simply perform parametric studies in an efficient way.

Two parametric studies have been performed:

- Measurement of the target length vs. SNR.
- Measurement of the target length vs. radial velocity.

In both cases: the measurement of the length has been performed on the integrated range profiles (both coherent and non-coherent), $\rho_r = 0.15\,\mathrm{m}$, $\rho_D = 2\,\mathrm{Hz}$, and $4\,\mathrm{m}$ of distance between both point scatterers of the synthetic target.

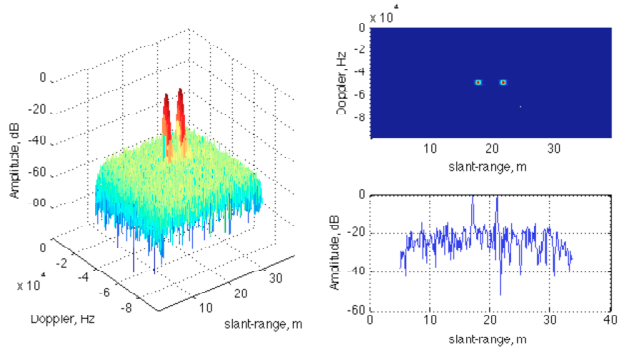

(a)

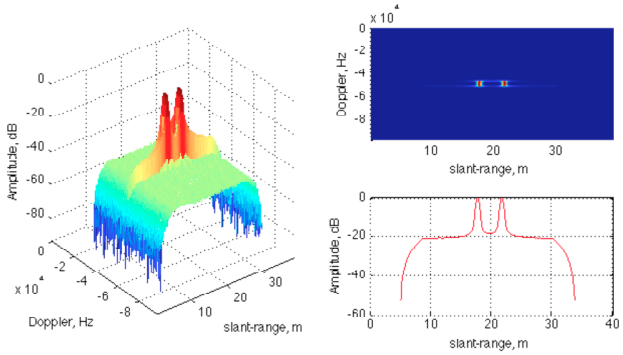

(b)

Figure 2. The I-Q range-Doppler integrated image and its range profile integrated in Doppler for the modelled two-point target. Left: 3D image; top right: 2D image; and bottom right: the I-Q integrated range profile. Target radial velocity 10 m/s, SNR = 21 dB. (a) the I-Q one, and (b) the non-coherent one. Note that the slant-range axes are set in relative units, not real position of the target, in order to get an easy measurement of the target length; also Doppler axes are set in relative units.

Figure 2(a) shows the I-Q range-Doppler integrated image and its range profile integrated in Doppler for the modelled two-point target. In the same way Figure 2(b) shows the non-coherent range-Doppler integrated image and its non-coherent range profile integrated in Doppler.

Note that the coherent integration of the image, of course, allows a better resolution of the target's hot spots to correct the range migration, eliminating the Doppler spreading effect. However, as shown in subsequent analysis, a greater precision in determining the target's dynamics is required, and it is much more sensitive to target scintillation due to the coherent summation of the scatterers from the target in the same range bin, an effect that does not occur with targets composed of point scatterers located in different resolution cells.

Table 1 shows the results of measurement of length, L, vs. SNR, performed on the integrated range profiles (both, I-Q and non-coherent) with the synthetic two-point scatterers target. The range of values chosen for the SNR was determined from a minimum value from which it might carry out measurements of length (the measure of the length was not possible with lower values of SNR), to a maximum from which length measurement is stabilized.

It is clear that best results for low SNR values are obtained for non-coherent integrated range profiles and range-Doppler images, whereas both procedures with high SNR can achieve similar results. In any case, since modelling is ideal, the results of Table 1 must be interpreted with caution and not always be extrapolated to real situations.

Table 1. Measurement of the target length vs. SNR, parametric study performed on the integrated range profiles (both, I-Q and non-coherent) with the two-point scatterers synthetic target. Target radial velocity 10 m/s.

	Target length (m)	
SNR, dB	I-Q	Non-coherent
0	6.822	4.019
3	13.360	4.019
6	11.030	4.019
9	2.430	4.019
12	4.112	4.019
15	4.019	4.019
18	4.112	4.019
21	4.112	4.019

Table 2. Measurement of the target length vs. radial velocity, parametric study performed on the integrated range profiles (both, I-Q and non-coherent) with the two-point scatterers synthetic target. SNR $= \infty$ dB.

	Target length (m)	
v_r, m/s	I-Q	Non-coherent
0	4.05	4.05
10	4.05	4.05
20	4.05	3.90
30	4.05	4.05
40	4.05	4.05
50	4.05	4.05
100	3.90	2.85
340	3.90	0.90

Table 2 shows the results of the study on the measurement of the target length, L, vs. radial velocity for the two-point scatterers target. The first simulated value of the radial velocity was 0, meaning the target is not moving, and the final value was 340 m/s (speed close to Mach 1 at Standard Sea Level conditions), in this way most of the situations of traffic surveillance scenarios were covered.

The target movement means that, during the time interval in which data are collected to form each one of the range-Doppler images of the sequence, the detected target may suffer the effects of range migration and Doppler spreading, quoted above. Furthermore, if the speed of the target is very high, there may be ambiguity in determining the target velocity with the radar system, and it can cause shifts in the range-Doppler image of the target (re-appearing the target in the radar image into the lower Doppler frequency area) As in the simulated case of the highest speed target. This latter effect is easily corrected.

It is straightforward to check that, as the radial velocity of the target is increased, the range-Doppler radar image of the target also the Doppler spreading effect is also increased, Figure 3, as a result of the range migration effect, within the non-coherent integrated range profiles. Conversely, the I-Q integrated range profiles are not affected by this effect, because the range migration is appropriately compensated. This fact implies that it is better to work with coherent range profiles and images when the speed of the target is increased.

On the other hand, for low values of SNR the coherent integration does not provide good results. Therefore, to solve this problem,

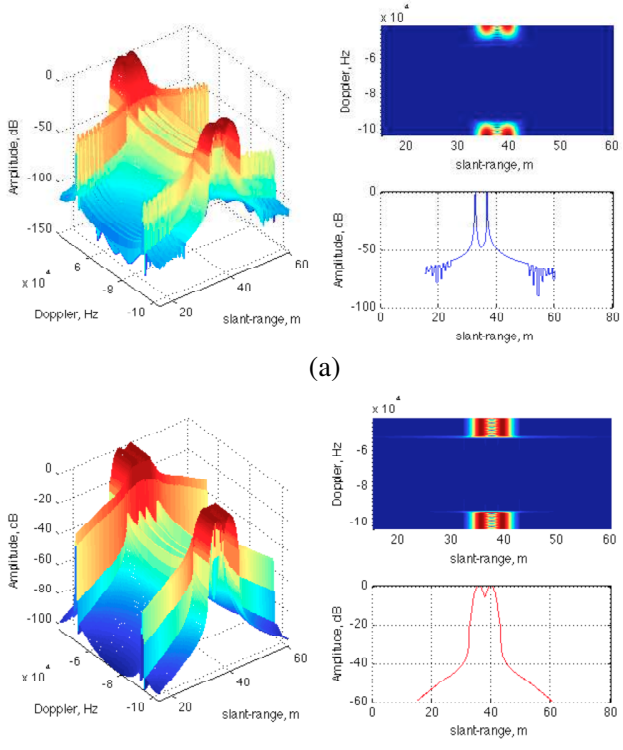

Figure 3. The modelled two-point scatterers target, with $v_r = 50\,\mathrm{m/s}$ and SNR $= \infty\,\mathrm{dB}$. (a) Left: the 3D I-Q range-Doppler integrated image; top right: 2D image; bottom right: the I-Q integrated range profile in Doppler. (b) Left: the 3D non-coherent integrated range-Doppler image; top right: 2D image; bottom right: the non-coherent integrated range profile in Doppler.

the capture parameters and the processing of the targets should be modified. This would not be desirable in scenarios with moving targets at very different speeds, such as the case of war scenarios with tanks (low-speed targets) and ground-ground missiles (high-speed targets).

4. EXPERIMENTAL RESULTS

Finally, we present the resulting data processing assessment using opportunity traffic, at different types of scenarios. Targets and scenarios presented are: a helicopter approaching, air traffic scenario

(a)

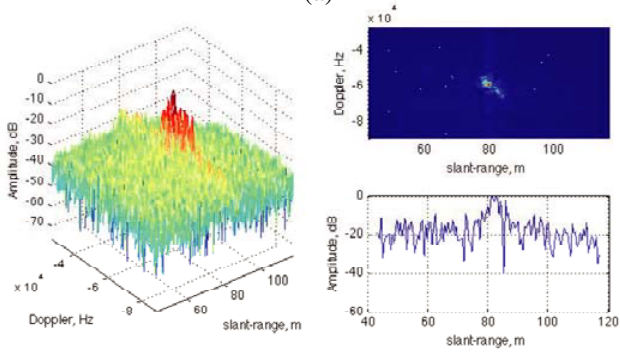

(b)

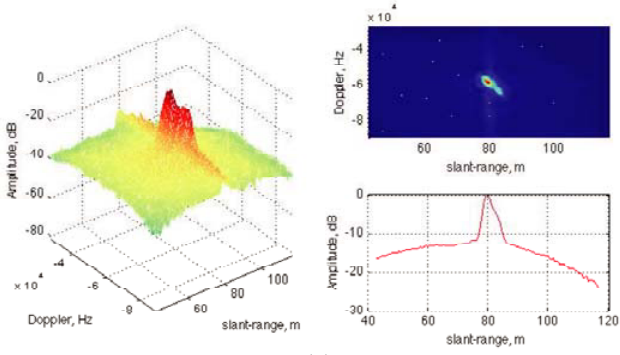

(c)

Figure 4. (a) Picture of the BK-117 helicopter (from the EUROCOPTER manufacturer). (b) Left: the 3D I-Q range-Doppler integrated image; top right: 2D image; bottom right: the I-Q integrated range profile in Doppler. (c) Left: the 3D non-coherent integrated range-Doppler image; top right: 2D image; bottom right: the non-coherent integrated range profile in Doppler.

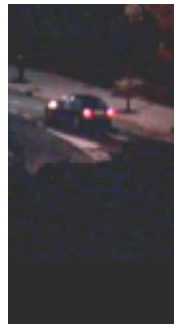

(a)

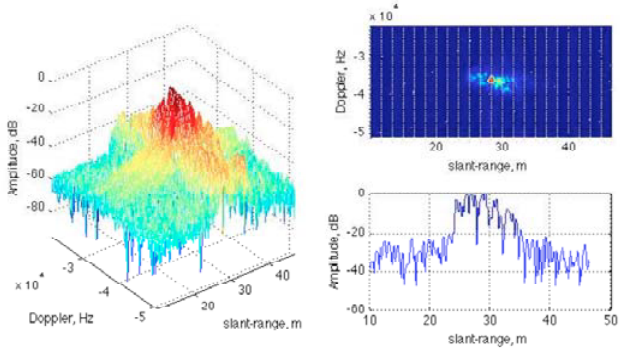

(b)

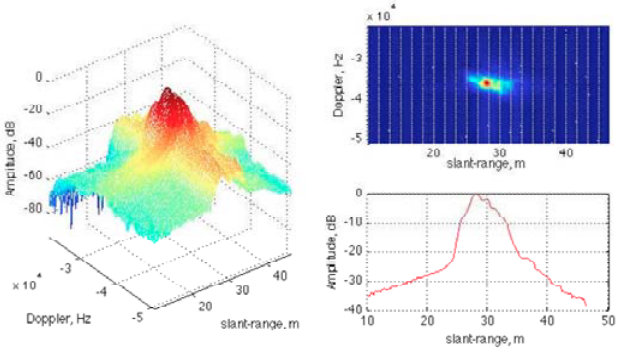

(c)

Figure 5. (a) Picture of the car. (b) Left: the 3D I-Q range-Doppler integrated image; top right: 2D image; bottom right: the I-Q integrated range profile in Doppler. (c) Left: the 3D non-coherent integrated range-Doppler image; top right: 2D image; bottom right: the non-coherent integrated range profile in Doppler.

(a)

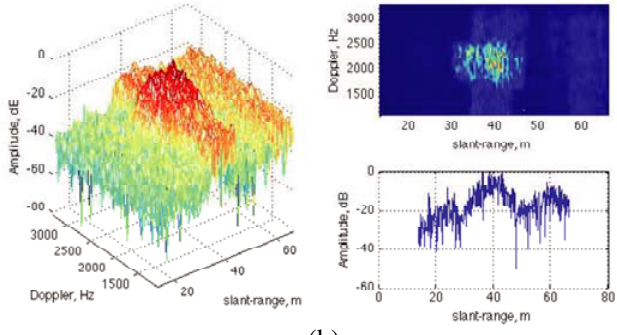

(b)

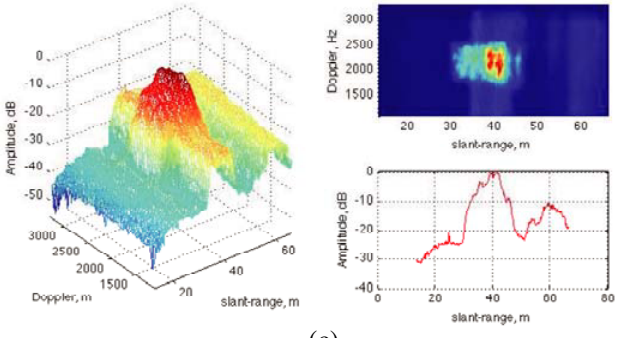

(c)

Figure 6. (a) Picture of the "Guardia Civil" patrol boat. (b) Left: the 3D I-Q range-Doppler integrated image; top right: 2D image; bottom right: the I-Q integrated range profile in Doppler. (c) Left: the 3D non-coherent integrated range-Doppler image; top right: 2D image; bottom right: the non-coherent integrated range profile in Doppler.

(Figure 4), a car captured at night conditions, road traffic scenario (Figure 5), a patrol boat of the "Guardia Civil" Spanish police

(a)

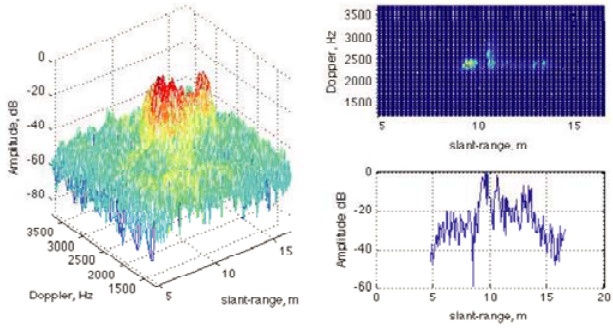

(b)

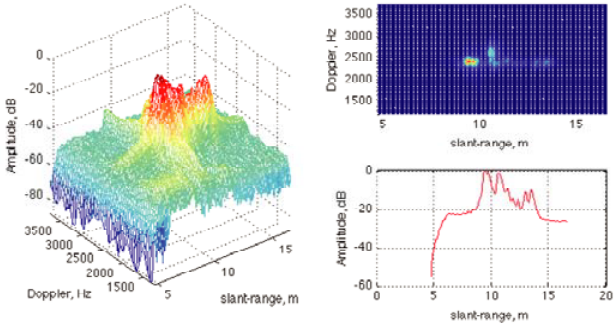

(c)

Figure 7. (a) Picture of the zodiac boat. (b) Left: the 3D I-Q range-Doppler integrated image; top right: 2D image; bottom right: the I-Q integrated range profile in Doppler. (c) Left: the 3D non-coherent integrated range-Doppler image; top right: 2D image; bottom right: the non-coherent integrated range profile in Doppler.

(Figure 6) and one zodiac boat (Figure 7), the latter two within a marine traffic scenario. In order to serve the purposes of extracting

Table 3. Experimental results on target length measurement.

Target	L_r, m	x, m/s	v_r, m/s	a, m/s^2
Helicopter	7.91	1314.31	−30.2612	2.667
Car	3.63	249.80	8.3542	0.941
Patrol boat	13.58	1970.02	−1.1150	0.107
Zodiac boat	4.48	616.65	1.1630	−0.013

L_r: radial length, x: slant-range (relative location of the target from de radar), v_{ri}: initial radial velocity (negative sign means the target is approaching), a: mean acceleration (including all acceleration components; negative sign means the target speed is decreasing).

and identifying characteristics of targets, the integrated range-Doppler image, the integrated range profile, its length measurement, from the integrated range profiles, the slant-range, the instantaneous initial radial velocity, and the mean acceleration were computed for each target (Table 3).

Table 3 presents the summary of the measured parameters for each of the considered targets. The showed measurement of the radial length of each target has been computed from the non-coherent integrated range profiles, for the four targets. This is due to, in the four cases, the SNRs are high enough and, as previously indicated, the length measurement gives a result almost the same performing the measurement both on the I-Q and on the non-coherent integrated range profiles, under these conditions.

The values obtained for the length of the presented targets are consistent with reality, including the lengthening produced by the wake pattern because of the water around the patrol boat. To make this comparison the fact that the measured length is the radial length should be considered. In the four cases presented, the corrections to be performed are relatively small to get the real length of the targets. These corrections are due to the aspect angles (in other words, the angles formed between the LOS and the axis that defines the main dimension of the target, L). Similar comments may be made to the obtained results for the radial velocity and the acceleration.

All information collected, taking into account the operating environments of each of targets, would allow a classification of such targets within each of the categories belonging to each type of target, i.e., helicopters, cars, small boats, and dinghies (or inflatable dinghies, at a finer classification).

5. CONCLUSIONS

We have presented a simple target classification technique for HRRs, oriented to traffic surveillance applications at any scenario, which is computationally very efficient. The technique is based on the estimation of different descriptors from a range-Doppler image sequence: length, range, velocity, acceleration, integrated range-Doppler image, and integrated range profile, the two latter computed in both coherent and non-coherent integration. In turn, these descriptors can be the basis for the development of new techniques for target classification.

The technique has been applied in scenarios, with opportunity traffic (and therefore with the HRR sensor system located in an non-optimal position) in which, with real data, the potential of the technique was confirmed, especially in air and sea traffic surveillance scenarios, in which its behaviour is much more favourable.

The presented technique is straightforward applicable to non-coherent scanning HRR, where the only difference that the input set of images to process are a set of scanning images range-azimuth, instead of the set of frames range-Doppler (as the presented case). Currently we are making some experiments with data from the ARIES radar [45], a surface surveillance HRR, in X-band, developed by Indra Sistemas, S. A. together with our research group.

ACKNOWLEDGMENT

This work was supported by the Project TEC2008-02148/TEC of the National Board of Scientific and Technology Research.

REFERENCES

1. Jonson, J., "Analysis of image forming systems," *Proc. Image Intensifier Symposium*, AD220160, 273–249, US Army Engineer Research and Development Laboratories, Fort Belvoir, VA, 1958.
2. Hovanessian, S. A. *Introduction to Sensor Systems*, Artech House Publishers, 1988.
3. Wehner, D. R., *High-Resolution Radar*, 2nd Edition, Artech House Publishers, 1995.
4. González, R. C. and R. E. Woods, *Digital Image Proccesing*, 3rd Edition, Addison Wesley Publishing Company, 2008.
5. Chang, Y.-L., C.-Y. Chiang, and K.-S. Chen, "SAR image

simulation with application to target recognition," *Progress In Electromagnetics Research*, Vol. 119, 35–57, 2011.

6. Woo, J.-C., B.-G. Lim, and Y.-S. Kim, "Modification of the recursive sidelobe minimization technique for the range-doppler algorithm of SAR imaging," *Journal of Electromagnetic Waves and Applications*, Vol. 25, No. 13, 1783–1794, 2011.
7. Lim, S.-H., C. G. Hwang, S.-Y. Kim, and N.-H. Myung, "Shifting MIMO SAR system for high-resolution wide-swath imaging," *Journal of Electromagnetic Waves and Applications*, Vol. 25, No. 8–9, 1168–1178, 2011.
8. Park, J.-I. and K.-T. Kim, "A comparative study on ISAR imaging algorithms for radar target identification," *Progress In Electromagnetics Research*, Vol. 108, 155–175, 2010.
9. Park, S.-H., M.-G. Joo, and K.-T. Kim, "Construction of ISAR training database for automatic target recognition," *Journal of Electromagnetic Waves and Applications*, Vol. 25, No. 11–12, 1493–1503, 2011.
10. Moreels, P. and S. E. Smrekar, "Watershed identification of polygonal patterns in noisy SAR images," *IEEE Transactions on Image Processing*, Vol. 12, No. 7, 740–750, 2003.
11. Wang, C. L., X. Fan, H. Guo, and J. Liao, "Identification of landslides in the Yangtze Gorges area of China using Radarsat and Chinese airborne L-SAR data," *Proc. IEEE International Geoscience and Remote Sensing Symposium*, Vol. 7, 3228–3230, Honolulu, HI, USA, 2000.
12. Chiang, H. C., O. L. Moses, and L. C. Potter, "Model-based classification of radar images," *IEEE Transactions on Information Theory*, Vol. 46, No. 5, 1842–1854, 2000.
13. Datcu, M., K. Seidel, and M. Walessa, "Spatial information retrieval from remote-sensing images. I. Information theoretical perspective," *IEEE Transactions on Geoscience and Remote Sensing*, Vol. 36, No. 5, 1431–1445, 1998.
14. Musman, S., D. Kerr, and C. Bachmann, "Automatic recognition of ISAR ship images," *IEEE Transactions on Aerospace and Electronic Systems*, Vol. 32, No. 4, 1392–1404, 1996.
15. Principe, J. C., M. Kim, and M. Fisher, "Target discrimination in synthetic aperture radar using artificial neural networks," *IEEE Transactions on Image Processing*, Vol. 7, No. 8, 1136–1149, 1998.
16. Li, J. and H. Ling, "Application of adaptive chirplet representation for ISAR feature extraction from targets with rotating parts," *IEE Proceedings on Radar, Sonar and Navigation*, Vol. 150, No. 4,

284–291, 2003.

17. Fang, J., H. Meng, H. Zhang, and X. Wang, "A low-cost vehicle detection and classification system based on unmodulated continuous-wave radar," *Proc. IEEE Intelligent Transportation Systems Conference*, 715–720, Seattle, WA, USA, 2007.
18. Duarte, C. C., B. P. D. Naranjo, A. A. Lopez, and A. B. del Campo, "High resolution CWLFM radar for vessel detection and idenfication for maritime border security," *Proc. International Carnahan Conference on Security Technology*, 304–307, Las Palmas, Spain, 2005.
19. Aoki, M., "Imaging and analysis of traffic scene," *Proc. International Conference on Image Processing*, Vol. 4, 1–5, Kobe, Japan, 1999.
20. Vespe, M., C. J. Baker, and H. D. Griffiths, "Radar target classification using multiple perspectives," *IEE Proceedings on Radar, Sonar and Navigation*, Vol. 1, No. 4, 300–307, 2007.
21. Yang, J.-R., S. Hong, and D.-W. Kim, "A distance-compensated radar sensor with a six-port network for remote distinction of objects with different dielectric constants," *Journal of Electromagnetic Waves and Applications*, Vol. 24, No. 11–12, 1429–1437, 2010.
22. Guo, K.-Y., Q. Li, and X.-Q. Sheng, "A precise recognition method of missile warhead and decoy in multi-target scene," *Journal of Electromagnetic Waves and Applications*, Vol. 24, No. 5–6, 641–652, 2010.
23. Huang, C.-W. and K.-C. Lee, "Frequency-diversity RCS based target recognition with ICA projection," *Journal of Electromagnetic Waves and Applications*, Vol. 24, No. 17–18, 2547–2559, 2010.
24. Munoz-Ferreras, J. M., J. Calvo-Gallego, and F. Perez-Martinez, "Monitoring road traffic with a high resolution LFMCW radar," *Proc. IEEE International Radar Conference*, 973–977, Rome, Italy, 2008.
25. Asensio-Lopez, A., A. Blanco-del-Campo, J. Gismero-Menoyo, D. Ramirez-Moran, G. Torregrosa-Penalva, B. P. Dorta-Naranjo, and C. Carmona-Duarte, "High range-resolution radar scheme for imaging with tunable distance limits," *IEEE Electronics Letters*, Vol. 40, No. 17, 1085–1086, 2004.
26. Blanco-del-Campo A., A. Asensio Lopez, B. P. Dorta Naranjo, J. Gismero Menoyo, D. Ramirez-Moran, C. Carmona-Duarte, and J. L. Jimenez-Martin, "Millimeter-wave radar demonstrator for high resolution imaging," *Proc. First European Radar Conference*,

65–68, Amsterdam, Holland, 2004.

27. Perez-Martinez, F., J. Garcia-Fominaya, and J. Calvo-Gallego, "A shift and convolution technique for high-resolution radar images," *IEEE Sensors Journal*, Vol. 5, No. 5, 1090–1098, 2005.
28. Munoz-Ferreras, J. M., J. Calvo-Gallego, F. Perez-Martinez, A. Blanco-del-Campo, A. Asensio-Lopez, and B. P. Dorta-Naranjo, "Motion compensation for ISAR based on the shift and convolution algorithm," *Proc. IEEE Radar Conference*, 366–370, Verona, NY, USA, 2006.
29. Chen, V. C. and W. J. Miceli, "Simulation of ISAR imaging of moving targets," *IEE Proceedings on Radar, Sonar and Navigation*, Vol. 148, No. 3, 160–166, 2001.
30. Atkins, R. G., R. T. Shin, and J. A. Kong, "A neural network method for high range resolution target classification," *Progress In Electromagnetics Research*, Vol. 4, 255–292, 1991.
31. Han, S.-K., H.-T. Kim, S.-H. Park, and K.-T. Kim, "Efficient radar target recognition using a combination of range profile and time-frequency analysis," *Progress In Electromagnetics Research*, Vol. 108, 131–140, 2010.
32. Huang, C.-W. and K.-C. Lee, "Application of ICA technique to PCA based radar target recognition," *Progress In Electromagnetics Research*, Vol. 105, 157–170, 2010.
33. Lee, K.-C., C.-W. Huang, and M.-C. Fang, "Radar target recognition by projected features of frequency-diversity RCS," *Progress In Electromagnetics Research*, Vol. 81, 121–133, 2008.
34. Lee, K.-C., J.-S. Ou, and M.-C. Fang, "Application of SVD noise-reduction technique to PCA based radar target recognition," *Progress In Electromagnetics Research*, Vol. 81, 447–459, 2008.
35. Seo, D.-K., K.-T. Kim, I.-S. Choi, and H.-T. Kim, "Wide-angle radar target recognition with subclass concept," *Progress In Electromagnetics Research*, Vol. 44, 231–248, 2004.
36. Li, H. J. and K. M. Li, "Application of wavelet transform in target identification," *Progress In Electromagnetics Research*, Vol. 12, 57–73, 1996.
37. Toribio, R., J. Saillard, and P. Pouliguen, "Identification of radar targets in resonance zone: E-pulse techniques," *Progress In Electromagnetics Research*, Vol. 43, 39–58, 2003.
38. Singh, A. K., P. Kumar, T. Chakravarty, G. Singh, and S. Bhooshan, "A novel digital beamformer with low angle resolution for vehicle tracking radar," *Progress In Electromagnetics Research*, Vol. 66, 229–237, 2006.

39. Wang, X., J.-F. Chen, Z.-G. Shi, and K. S. Chen, "Fuzzy-control-based particle filter for maneuvering target tracking," *Progress In Electromagnetics Research*, Vol. 118, 1–15, 2011.
40. Shi, Z.-G., S.-H. Hong, and K. S. Chen, "Tracking airborne targets hidden in blind doppler using current statistical model particle filter," *Progress In Electromagnetics Research*, Vol. 82, 227–240, 2008.
41. Haridim, M., H. Matzner, Y. Ben-Ezra, and J. Gavan, "Cooperative targets detection and tracking range maximization using multimode ladar/radar and transponders," *Progress In Electromagnetics Research*, Vol. 44, 217–229, 2004.
42. Jia, Y., L. Kong, and X. Yang, "A novel approach to target localization through unknown walls for through-the-wall radar imaging," *Progress In Electromagnetics Research*, Vol. 119, 107–132, 2011.
43. Conceição, R. C., M. O'Halloran, E. Jones, and M. Glavin, "Investigation of classifiers for early-stage breast cancer based on radar target signatures," *Progress In Electromagnetics Research*, Vol. 105, 295–311, 2010.
44. Conceição, R. C., M. O'Halloran, M. Glavin, and E. Jones, "Evaluation of features and classifiers for classification of early-stage breast cancer," *Journal of Electromagnetic Waves and Applications*, Vol. 25, No. 1, 1–14, 2011.
45. Pérez, F., A. Asensio, J. Gismero, J. I. Alonso, J. M. Monje, F. Casanova, R. Cortijo, and J. F. Perez-Ojeda, "ARIES: A high resolution shipboard radar," *Proc. IEEE Radar Conference*, 148–153, Long Beach, CA, USA, 2002.